

# **Numerical Crack Growth Analysis in AA2024-T3 Friction Stir Welded Butt Joints**

**P. Carlone, R. Citarella, M. Lepore and G.S. Palazzo**  
**Department of Industrial Engineering**  
**University of Salerno, Fisciano (SA), Italy**

## **Abstract**

This paper deals with a numerical investigation on the influence of residual stresses on fatigue crack growth in AA2024-T3 friction stir welded butt joints. The computational approach is based on the coupled usage of the finite element method (FEM) and the dual boundary element method (DBEM), in order to take advantage of the main capabilities of the two methods. Linear elastic FE simulations are performed to evaluate the process induced residual stresses, by means of the “contour method” technique. The computed stress field is then superimposed on the stress field produced by a remote fatigue traction load applied on a cracked specimen, and the crack propagation is simulated in a DBEM environment, according to a two-parameters growth model. The results obtained highlight the influence of the residual stress distribution on crack growth.

**Keywords:** friction stir welding, residual stress, contour method, two parameters crack growth model, FEM-DBEM approach

## **1 Introduction**

Friction stir welding (FSW) is an innovative joining technique patented by The Welding Institute of Cambridge in 1991. Conceptually, the FSW process is quite simple: a non-consumable rotating tool, constituted by a shoulder and a pin, is inserted between the adjoining edges of the parts to be welded and moved along the desired weld line. The tool movements lead to a local increase of the work piece temperature, with heat generation, caused by frictional effects and plastic deformation; as a consequence the induced softening allows the processing material to flow around the pin, according to complex patterns, resulting into a solid state weld [1-3]. Since its development, the FSW process has been more and more applied in several sectors, such as aeronautical, automotive, and nautical among others; moreover, much effort has been spent by several research groups worldwide

to provide a deeper understanding of process effects on mechanical properties, microstructure, and residual stress induced by the process [4-9].

One of the reasons justifying the deep industrial, as well as academic interest in FSW is related to the remarkable advantages connected to solid state welds provided by this technique. During the process, the material is heated below the melting temperature and, as a consequence, all phase transformations happen at the solid state. This feature makes the FSW process very promising in joining difficult-to-weld materials, such as the 2XXX and 7XXX aluminum series, generally considered as non-weldable using conventional techniques, due to the relatively high porosity in the melting zone, resulting into significant mechanical property impairment with respect to the base materials [4-6].

A wider implementation of the technique in safety-critical components, however, requires a deeper understanding of fatigue behavior of FSWed assemblies. In this sense some results have already been presented in the inherent literature, relatively, for instance, to AA6082-T6 and AA6061-T6 [10], AA6063-T6 [11], AA2024-T351 [12], AA6005C [13], and AA2915 [14] FSW joints. The slower crack propagation in FSWed material with respect to the base material has been highlighted in [10-12] and related to microstructure, microhardness, and residual stress. An extensive experimental study on the fatigue strength of FSWed AA6005C butt joints has been reported in [13], considering also the influence of the inclination of the applied cyclic stress with respect to the weld line. The obtained results highlighted a variation of the localization of the initial crack with respect to the loading inclination and to the presence of welding flash, and a negligible influence of the same parameters on fatigue strength. The key role of process induced residual stresses on crack growth of FSWed assemblies has also been evidenced in [14]. In the same work a significant reduction of crack growth rates can be obtained by means of a laser peening treatment on welded specimens, whereas negligible benefits are provided by the conventional shot peening process.

Even if FSW residual stresses are generally lower if compared to conventional welding processes [15], an accurate knowledge of the process-induced residual stresses is highly desired to numerically predict fatigue behavior of welded products as well as to analyze experimental crack growth tests. Several approaches to the evaluation of FSW induced residual stresses have been proposed in literature, based both on numerical [16] and experimental techniques [17,18], revealing a tensile stress status in correspondence of the welding line balanced by compressive stress in the base material. An asymmetric longitudinal stress distribution, with a tensile peak in the weld zone in correspondence of the advancing side, has been evidenced in [17] by means of synchrotron X-ray diffraction analysis, whereas some through the thickness variations of the longitudinal stress have been measured using the hole-drilling strain gauge method in AA2219-T62 FSW butt joints [18].

In this paper a numerical investigation on the influence of residual stresses, induced by the friction stir welding process, on fatigue crack growth in AA2024-T3 butt joints has been proposed. The computational approach is based on the coupled usage of finite element method (FEM) and dual boundary element method (DBEM). In particular, linear elastic FE simulations have been performed to evaluate the process induced residual stresses, by means of a recently developed technique

named “Contour Method”, which is based on the combination of experimental procedures and numerical calculations. The computed residual stress field is then superimposed to the stress field produced by a remote fatigue traction load and a crack propagation is simulated by the dual boundary element method (DBEM) [19] in an automatic way. A two-parameter crack growth law is used for the crack propagation rate assessment [20]. The DBEM code BEASY and the FEM code ANSYS are coupled in the aforementioned numerical approach by in house developed routines.

The paper has been organized as follows: in Section 2, details relative to used material, FSW performed process, application of the “Contour Method”, and simulation of the crack growth are provided, while, in Section 3 the obtained results are presented and discussed. Finally, in Section 4, the most relevant conclusions are outlined.

## 2 Materials and Methods

### 2.1 Materials and Process Details

The friction stir welding process, in the most general case, is based on three different stages: the plunge stage, consisting into the penetration of the tool pin into the processing material in correspondence of the adjoining edges, including eventually also a dwell period in order to sufficiently preheat the material; the welding stage, characterized by the travel of the rotating tool along the desired weld line; the tool extraction form the material at the end of the process. The process is influenced by several parameters, such as processing material, tool geometry, rotating and travelling speeds, pin penetration and tilt angle, as shown in Fig 1a).

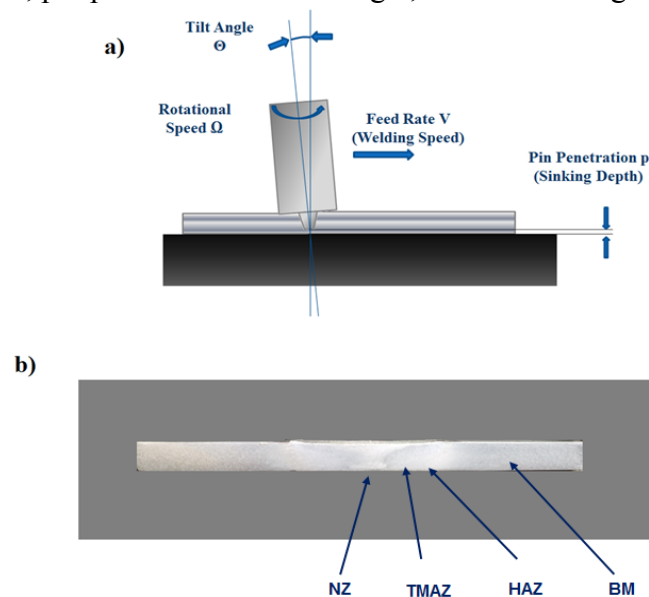


Figure 1. Friction stir welding process scheme a) and macroscopic observation of the weld section b)

During the welding process, heat generation related to frictional effects and material stirring results into a local increase of the workpiece temperature. The subsequent softening allows the processing material to flow from the front to the back of the tool, forced by the rotation of the pin, resulting into a solid state weld. Temperature increase and plastic deformation leads to the formation of micro-structurally different zones: the nugget zone (NZ) in the centre of the weld, characterized by a grain refinement, surrounded by a thermo-mechanical affected zone (TMAZ) and a heat affected zone (HAZ), as can be seen in Fig. 1b). A complete knowledge of the flow patterns during the FSW process has not been achieved yet, however, according to several models, the formation of the weld nugget is due to the extrusion of the material from the retreating side into a plasticized zone surrounding the pin [21].

The base material used in the present investigation was aluminium AA2024-T3 plate, having the following nominal composition: 3.8-4.9 Cu, 1.2-1.8 Mg, 0.3-0.9 Mn, 0.5 Si, 0.5 Fe, 0.25 Zn, 0.15 Ti, 0.1 Cr, balance Al (wt%). The considered material has been subjected to a solution heat treatment, followed by cold working and natural ageing. The Young modulus is equal to 70 GPa and the Poisson ratio  $\nu=0.3$ . Plate dimensions are: length 100 mm, width 30 mm, and thickness 4 mm. FSW processes have been executed on a machining center (MCX 600 ECO), using an opportunely realized clamping fixture, in order to fix the welding material according to the desired tilt angle. A full factorial design of experiments has been used, assuming five and three levels for the rotating speed  $\Omega$  (800, 1000, 1200, 1400, 1600 rpm) and feed rate  $V$  (35, 70, 140 mm/min), respectively. Other process parameters, i.e. tool geometry, tilt angle  $\Theta$ , and pin penetration  $p$ , have been defined by the means of preliminary tests and kept as constants in all experiments. The used tool consisted of a 20 mm diameter shoulder with a conical pin, characterized by the following dimensions: height 3.80 mm, diameter 6.20 mm, and cone angle  $30^\circ$ . The tool was made of AISI1040 quenched steel (56 HRC). The tilt angle and the pin penetration have been assumed equal to 2 degrees and 0.2 mm respectively. In Fig 2, the setup of the process is shown.

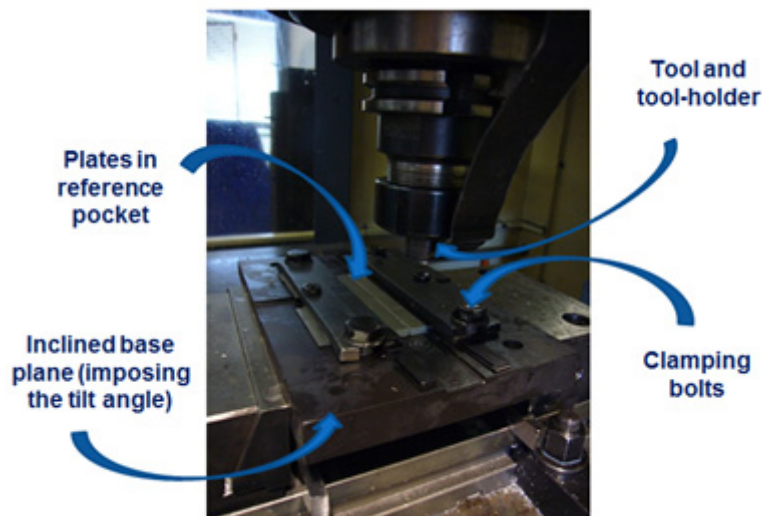


Figure 2. Friction stir welding process setup

## 2.2 Residual stress measurements

The “contour method”, recently proposed by Prime [22], is a relaxation method allowing the evaluation of the residual stress distribution on a specimen section; in particular only the normal component (in a direction orthogonal to the aforementioned plane) of such stresses can be considered. The most interesting capability of the method, if compared to other destructive technique, such as the *cut compliance method*, the *hole drilling*, and the *deep hole drilling*, is related to the possibility to obtain a complete mapping of the residual stresses, instead of an averaged or a local value, following a relatively simple and cheap procedure.

From a theoretical point of view, the “contour method” is a derivation of the Bueckner’s elastic superposition principle, which states an equivalence between the normal stresses to be applied on a specimen section in order to deform the surface to its initial undeformed shape and the normal residual stress acting on the same section before the cut. Validations of the “contour method” can be found in [22-25] where contour results are compared with data provided by neutron diffraction and synchrotron X-ray diffraction.

The application of the contour method is based on three consecutive steps: surface cut and stress relaxation, acquisition of the displaced surface, stress computation by finite element analysis. A schematic representation of the procedure applied in this investigation has been reported in Fig. 3.

In more details, after the friction stir welding process, samples have been opportunely polished and cut orthogonally to the welding line in correspondence of the middle length, by means of wire electrical discharge machining (WEDM), in order to avoid stresses due to sectioning, allowing the surface to freely relax and providing a surface characterized by reduced roughness. Moreover, to ensure a straight cut, the welded specimen has been rigidly clamped in correspondence of both opposite edges (Fig. 3 a and b).

WEDM process has been performed on a MITSUBISHI FA-20 machine, using a copper 0.25 mm diameter wire. Cut parameters have been assumed according to the predefined finishing mode. Each cut required about 15 min. In Fig. 3c, two halves of a welded specimen, after stress relaxation, are shown.

Displacements of the sectioned surfaces have been recorded using a Coordinate Measuring Machine, type DEA IMAGE GLOBAL CLIMA, using a contact probe, characterized by a 3 mm diameter ruby tip (Fig. 1d). A 0.5x0.5 spacing grid has been used for the acquisition of the out of plane displacements, resulting into about 1100 data points on each surface, in a reference coordinate system defined in Fig 1.e. Experimental data provided by the acquisition of surfaces relative to both halves of the cut specimen have then been combined and processed in the MATLAB environment, in order to fit the experimental data to a smoothing surface, improving the quality of the regression with respect to the polynomial surface fitting adopted by the same authors in [26].

The residual stress distribution has been finally obtained by means of an elastic FE model of the cut sample, using the measured and digitalized out of plane displacements, with reversed sign, as input nodal boundary conditions. The FE model has been solved using the commercial package ANSYS (Fig. 1g and 1h). The

Young modulus and the Poisson coefficient have been defined equal to 70 GPa and 0.3, respectively.

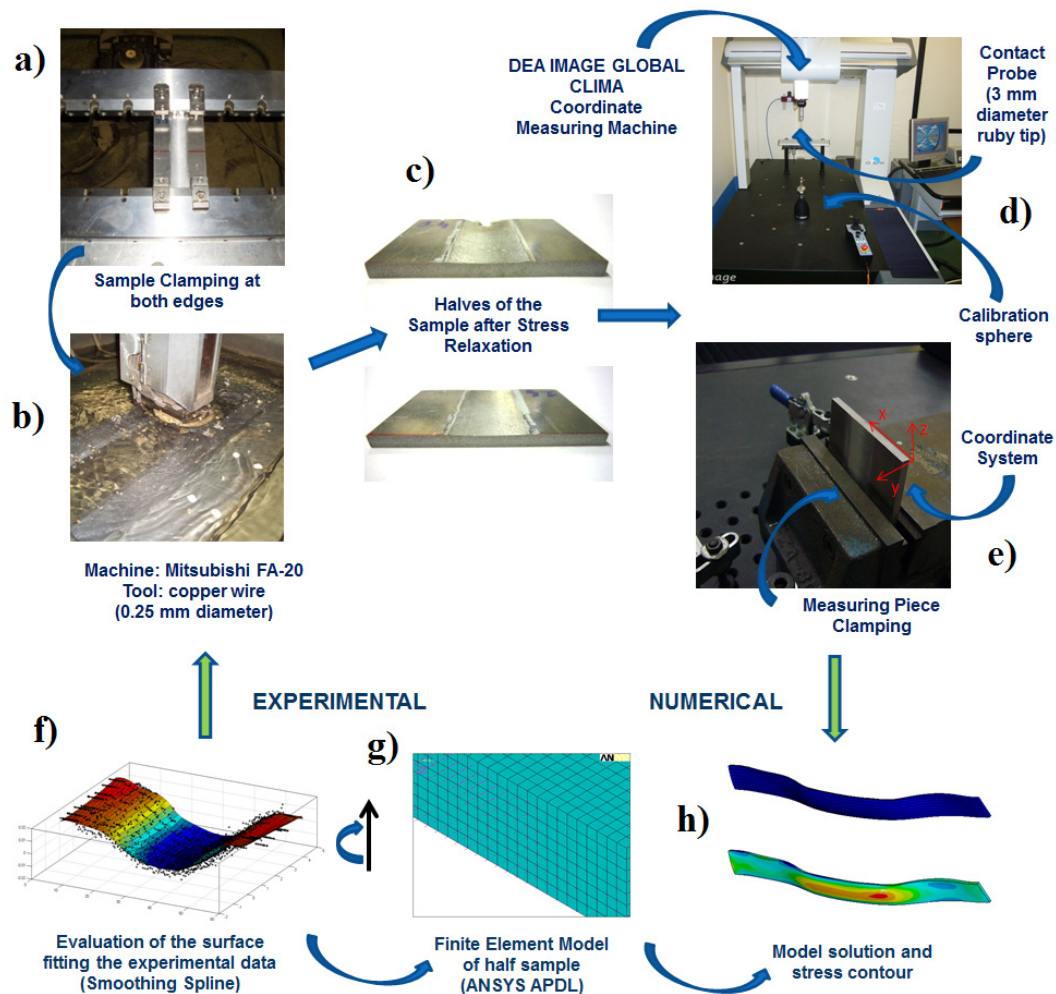


Fig. 3. a) sample clamping for the cutting process; b) WEDM cut of the joined pieces; c) detail of the cut sample; d) scanning of the cut surface by CMM; e) detail of the measuring sample; f) contour surface; g) FE model of the cut sample; h) normal residual stress distribution

## 2.3 DBEM Crack Propagation

### 2.3.1 Theoretical approach

The basic effect of residual stresses applied on the crack faces is to change the effective value of the total stress intensity factor (SIF) at the crack tip, with both  $K_{min}$  and  $K_{max}$  generally affected in the same way, so as to leave unchanged the parameter  $\Delta K$ . Consequently, the primary effects of residual stresses on crack growth rates are related to the  $K_{max}$  variations and not to the  $\Delta K$  variations. This is accounted for by the aforementioned two parameters approach[19, 27]: according to this theory,

fatigue crack growth can be viewed, fundamentally, as a two-parametric problem, where two driving forces,  $K_{max}$  and  $\Delta K$ , drive the growth of a fatigue crack. Since it is assumed that, in presence of an overload,  $K_{max}$  also enters as the major driving force for fatigue crack growth (in addition to the classical parameter,  $\Delta K$ ), the corresponding residual stresses can affect crack growth rates even if they do not affect the parameter  $\Delta K$ . In addition, the theory assumes that there are two fatigue thresholds,  $K_{max,th}^*$  and  $\Delta K_{th}^*$  corresponding to the two driving forces. These are asymptotic values in the  $\Delta K$ - $K_{max}$  graphs of the fatigue curves [27]: both the driving forces must be simultaneously larger than the relative thresholds for fatigue crack growth to occur. Since residual stress effects manifest primarily through a variation in  $K_{max}$  levels, a crack growth rate variation generally follows (an arrest in crack growth can occur if these stresses are compressive and sufficiently high to make the overall  $K_{max}$  fall below  $K_{max,th}$ ). The crack growth law is assumed as follows [27]:

$$\frac{da}{dN} = A (\Delta K - \Delta K_{th}^*)^n (K_{max} - K_{max,th}^*)^m \quad (1)$$

and is calibrated by best fitting the material parameters  $A$ ,  $n$ ,  $m$  based on constant amplitude preliminary test. The threshold parameters  $K_{max,th}^*$ ,  $\Delta K_{th}^*$  are also evaluated by experimental tests: it is important to note that the threshold parameters are strongly related with the microstructure of the considered alloy, since they are related to ‘microscopic’ crack growth rates, acting at the microstructure scale. The friction stir welding effects are reproduced by taking into account the residual stress influence on the driving parameters  $\Delta K$  and  $K_{max}$ .

### 2.3.2 Crack growth law fatigue parameters

It is remarkable that the two parameter crack growth law (Eq. 1), whose validity is expected to be extended to any overload ratio, is calibrated using only experimental data from constant amplitude test. The experimental threshold data and the material parameters ( $A$ ,  $n$ ,  $m$ ) for the considered material are obtained from literature [27]:

$$\begin{aligned} \Delta K_{th}^* &= 1834121 \text{ N/m}^{3/2} \\ K_{max,th}^* &= 3352014 \text{ N/m}^{3/2} \\ A &= 6.745\text{e-}23, \\ n &= 1.65, \\ m &= 0.50. \end{aligned}$$

having expressed  $da/dN$  in m/cycle and  $\Delta K$  in  $\text{N/m}^{3/2}$ . Such values are valid for every positive  $R$ -ratio [27].

The residual stress effects are evaluated by considering the crack growth law (Eq. 1), in which the SIF is defined by the sum of the nominal SIF, corresponding to the remote load, plus the SIF corresponding to the contribution of the residual stresses induced by the friction stir welding process (and applied on the crack faces).

### 2.3.3 Procedure description

The Bueckner approach is adopted as derived from an application of the superposition principle: it states that the residual stress effect on the SIFs can be equivalently modelled by a distribution of tractions applied on the advancing crack faces (Fig. 4). Such tractions are obtained from the residual stresses, imported by the FEM code, existing on the virtual surface traced by the advancing crack.

The following step is to realise a crack propagation analysis, with the stress intensity factors (SIFs) and crack growth rates calculated by DBEM [27], based on the chosen crack propagation law (Eq. 1). In particular, a CT (compact tension) specimen, with an initial crack undergoing the residual stresses imported by the FEM code ANSYS, is modelled by the BEASY code (Figs. 4-5). The mesh density is variable along the crack propagation (also depending on the chosen crack advance in the generic step of propagation) from 1494 to 3786 *reduced quadratic* elements (the node at the element centre is missing). The maximum crack advance at each step is varying from 0.5 mm, in the initial stage of crack propagation, to 1 mm in the final stage.

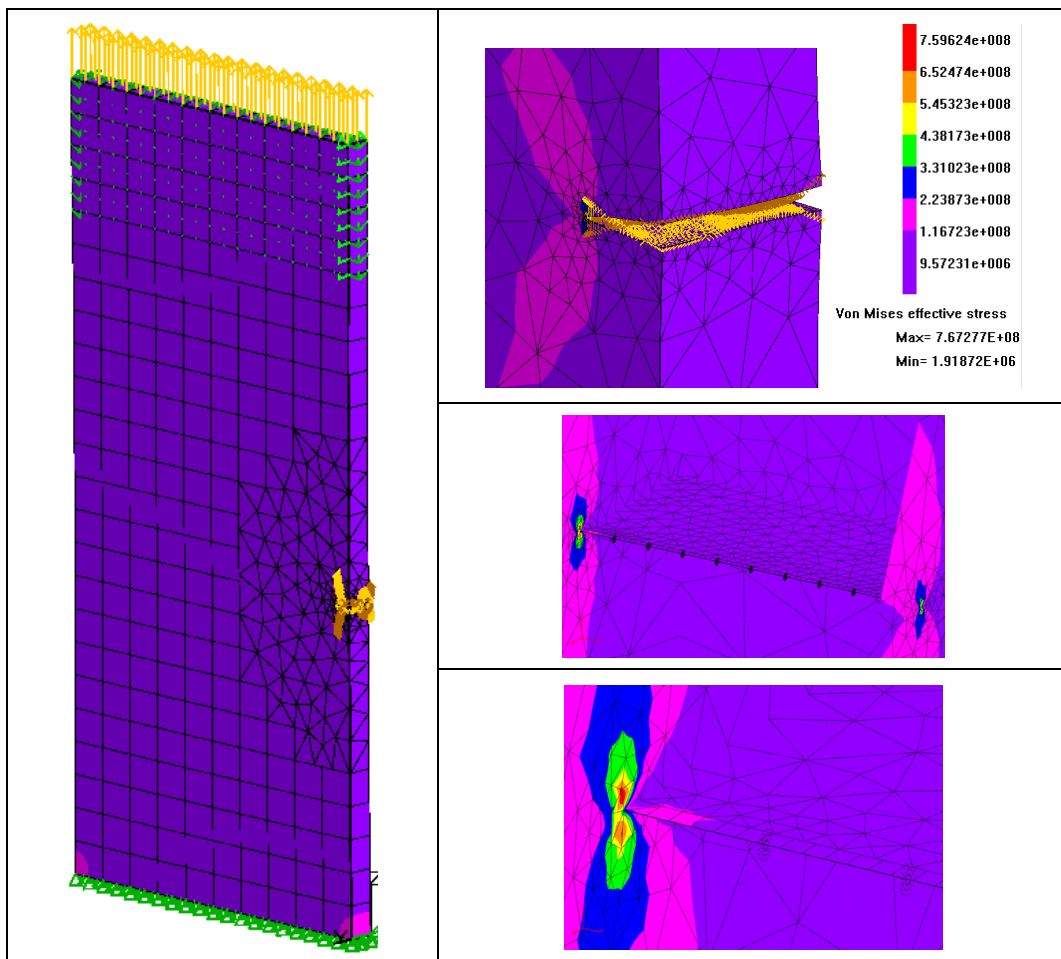


Fig. 4. Initial through crack introduced in the DBEM model with highlight of the Von Mises stresses [Pa], of the residuals stresses on the crack faces and of the j-path positioning along the crack front.

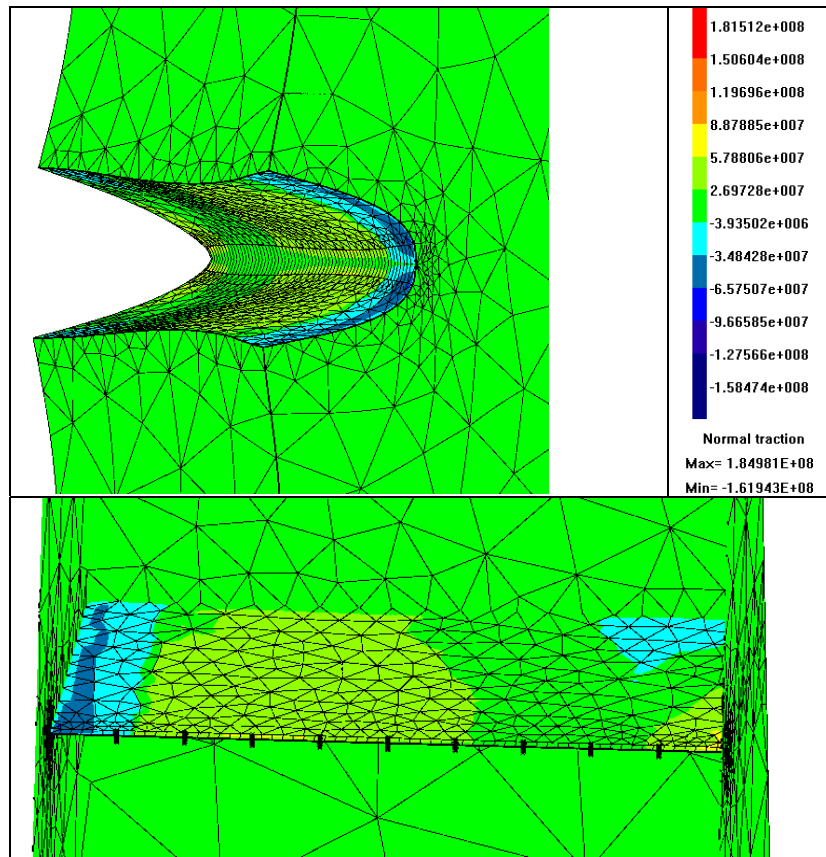


Fig. 5. Initial through crack with highlight of the residual stresses on the crack faces [Pa] (the opening tractions are negative).

Such specimen undergoes a maximum remote traction load equal to 24 kN, with a stress ratio  $R=0.1$ .

### 3 Results and Discussion

In this Section, relevant results obtained applying the developed FEM-DBEM approach are exposed and discussed. In particular, reported data refers to the sample welded assuming the rotational speed equal to 1400 rpm and the welding speed equal to 70 mm/min.

In Fig. 5 it is possible to see the deformed plot of the crack: it is clear the beneficial effect of the compressive residual stresses that reduces the crack opening in that part of the crack that during the propagation is crossing the compressive residual stress field.

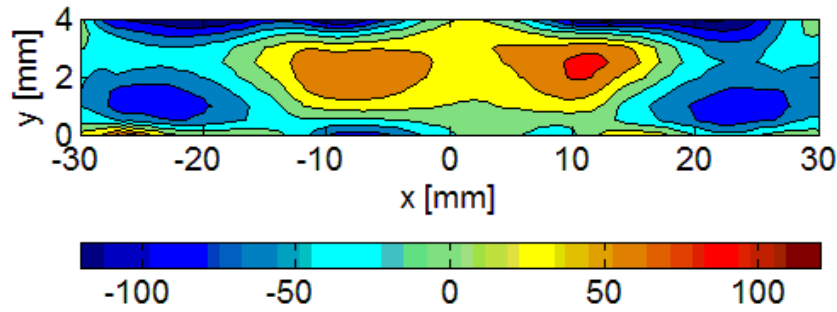


Fig. 6. Longitudinal residual stresses [MPa] distributions in the middle specimen section, as evaluated by the contour method ( $V = 70$  mm/min)

In Fig. 6 the longitudinal ( $z$  direction) residual stress distribution, evaluated applying the contour method, is shown, magnifying the sample thickness ( $y$  direction) for clarity. Reported result evidences a tensile residual stress status in correspondence of the weld line, balanced by compressive stresses on the two sides of the weld. Two different tensile peaks have been found in the stress distribution, localized at a distance from the weld center equal to the shoulder radius into the advancing and retreating sides. In particular, the largest tensile stress, equal to 100 MPa, has been detected in the advancing side, below the top surface, in agreement with other reports [16-18], whereas the tensile peak in the retreating side resulted equal to about 90 MPa. Furthermore, some asymmetries in the stress distribution can be observed, easily explainable taking into account the different relative velocities between the advancing and the retreating sides.

Line plots of the longitudinal residual stresses have been reported in Fig. 7, evidencing the stress variation in the mid thickness of the sample and along the thickness direction in correspondence of the weld line center and of the tool radius of both sides of the weld. As can be seen compressive stresses have been found also in correspondence of the top and bottom surface of the welded sample, changing to tensile at a distance from the external surface of about 0.5 mm. A relatively less severe stress profile has been computed at the center of the weld line.

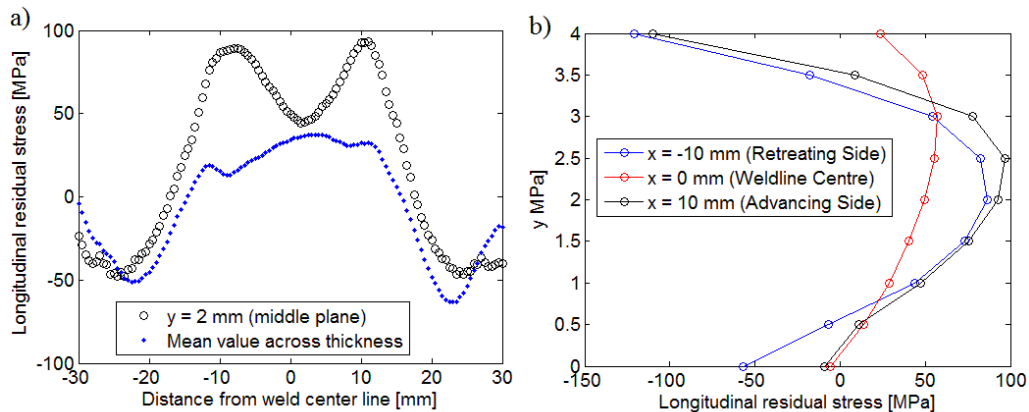


Fig. 7. a) longitudinal stress profiles and b) stress profiles along the thickness.

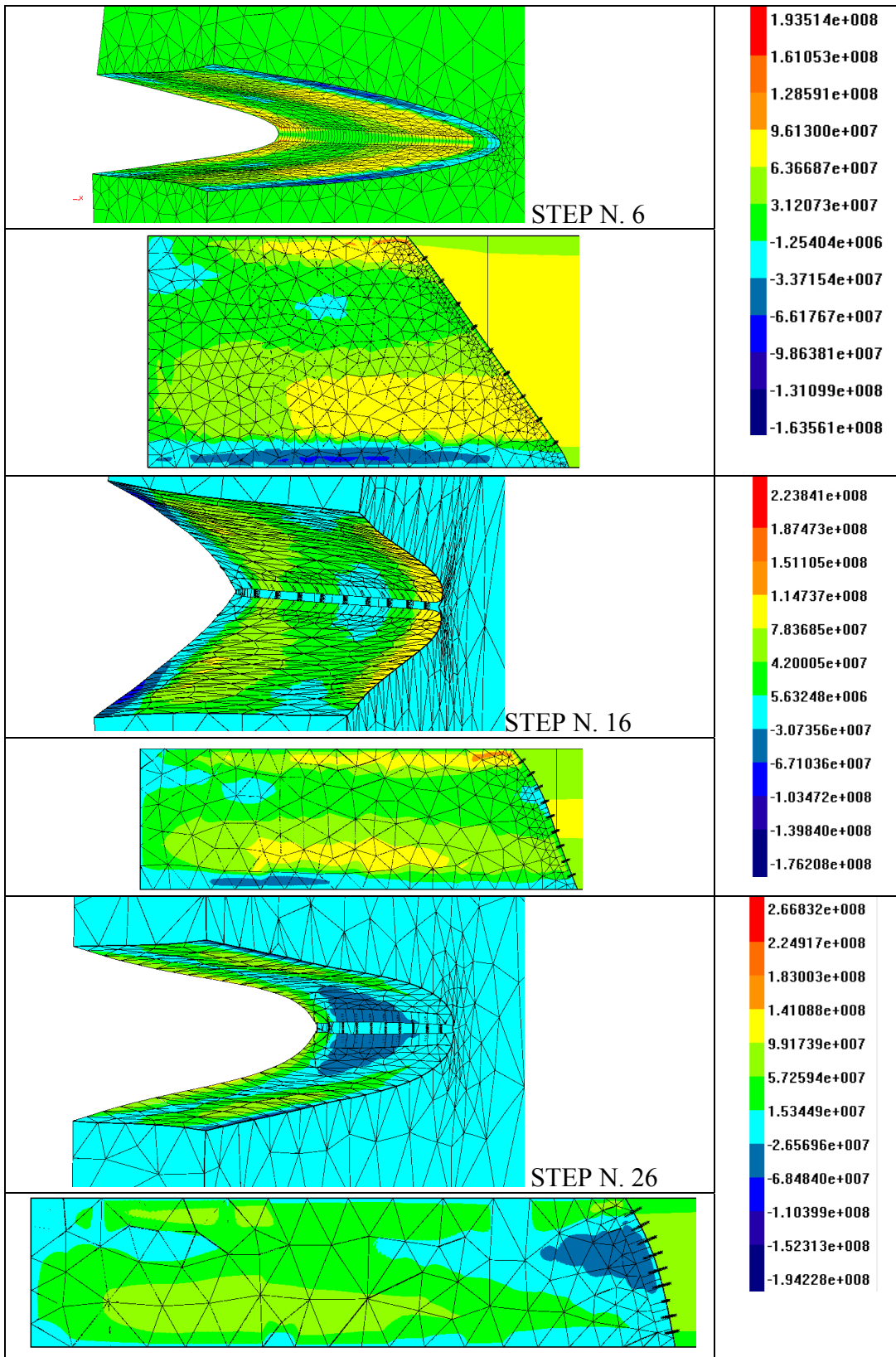


Fig. 8a. Advancing crack fronts with highlight of normal tractions [Pa].

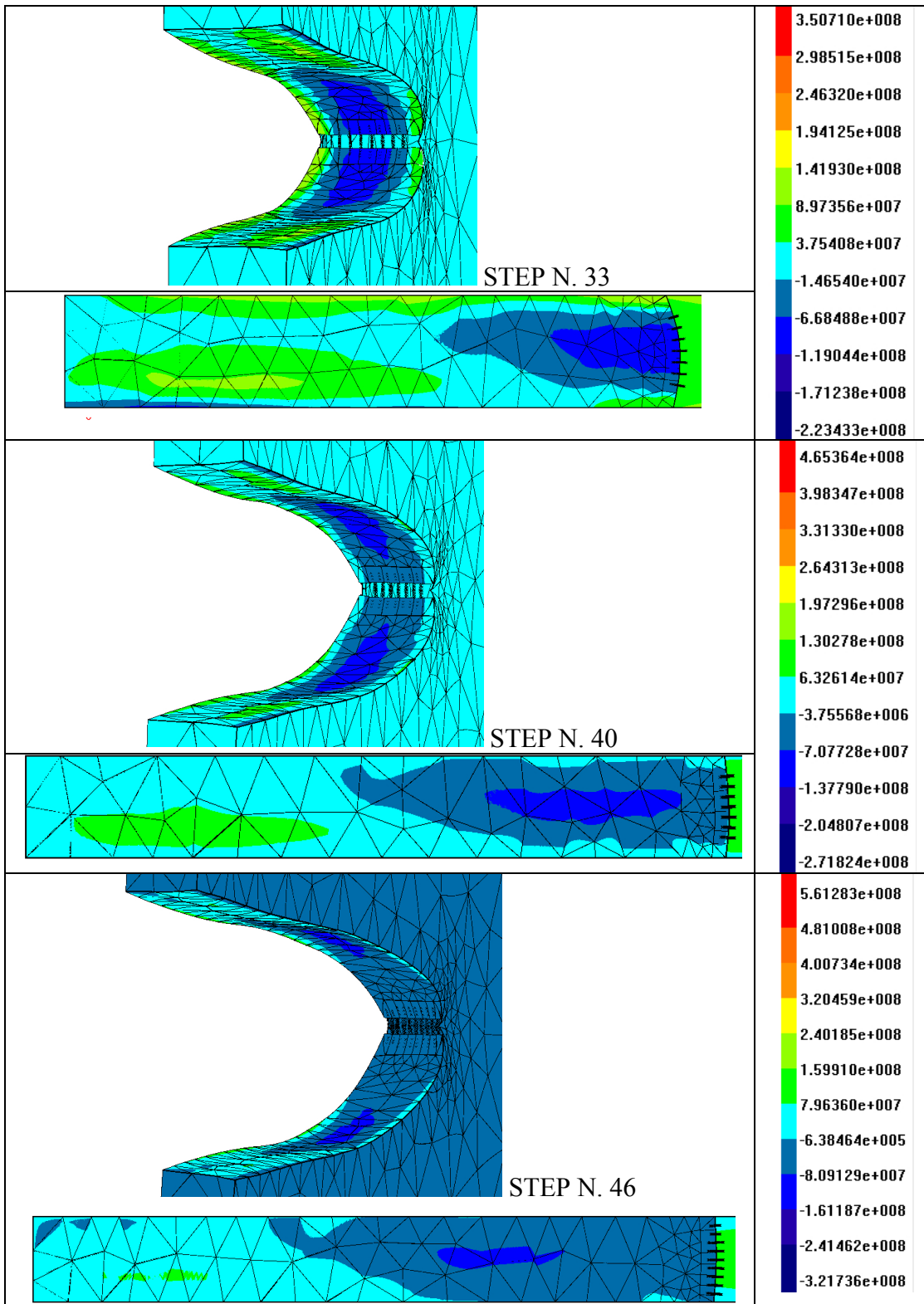


Fig. 8b. Advancing crack fronts with highlight of normal tractions [Pa].

In Figures 8a-b the propagating crack is showed at different growth steps: the peculiar crack face deformation is clearly to be related to the residual stresses in addition to the remote load. The corresponding KI values along the crack front, calculated by the J-integral technique [27], are showed in Fig. 9 at different crack increments. The crack size, measured at three points of the crack front (the two break through points A, C and the centre point B), is shown against the number of fatigue cycles in Fig. 10. The propagation proceeds under pure mode I, because the residual stresses imported from FEM are only those perpendicular to the crack face.

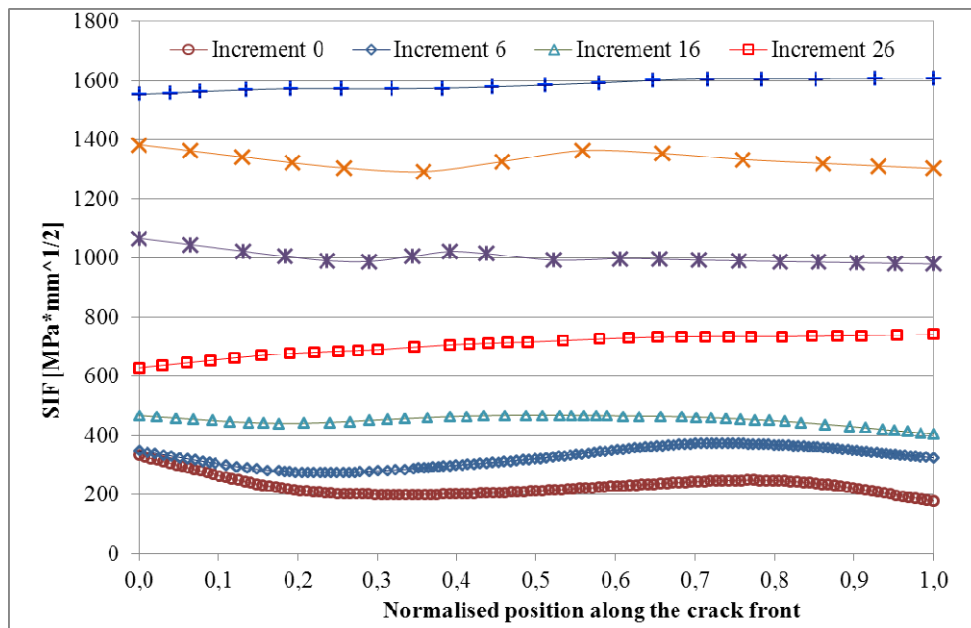


Fig. 9. KI values along the crack front at different increments.

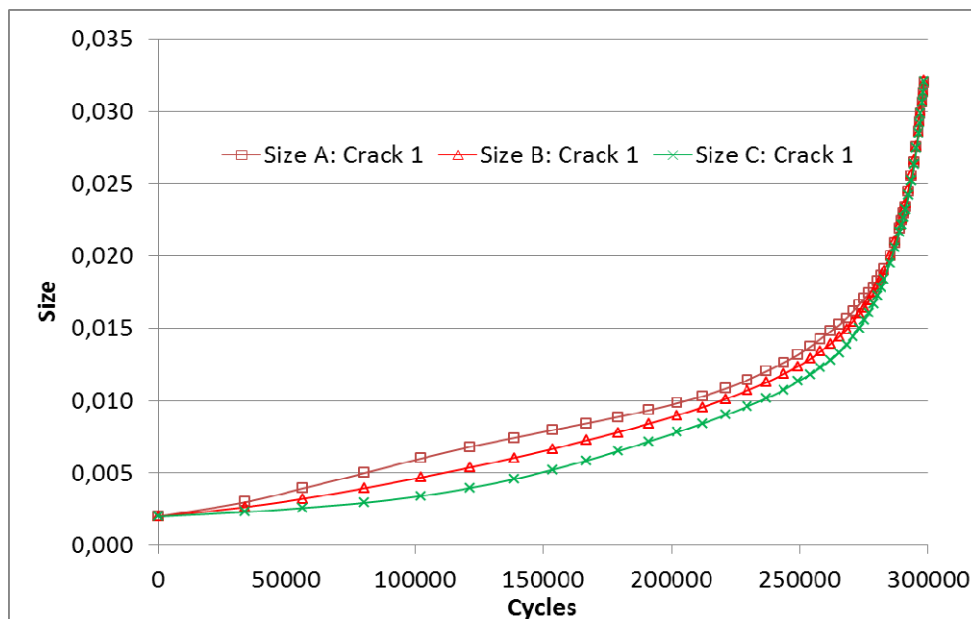


Fig. 10. Crack size [m] against number of cycles.

## 4 Conclusions

Taking into account the results presented in this paper, the following conclusions can be highlighted:

- An asymmetric stress distribution, characterized by tensile stress in correspondence of the weld line, balanced by compressive stresses into the contiguous material, has been found;
- The tensile stress peak has been localized in the advancing side and below the top surface (loaded in compression);

Moreover, the residual stress effect on crack growth rates and on crack shape, depends on the following material parameters:

- The stress-strain curve (that affects the FEM calculations of the residual stress);
- The thresholds  $\Delta K_{th}^*$  and  $K_{max,th}^*$  of the driving forces;
- The constant amplitude crack growth curves.

It is to point out the extreme flexibility and efficiency of the methodology adopted, because the two methodologies (FEM and DBEM) are complementary for such kind of problems: FEM can be adopted for the visco-plastic analysis, needed to simulate the FSW process and calculate the residual stresses (as an alternative to the contour method), whereas the accuracy typical of the DBEM applied to fracture mechanics is well known, with the three dimensional crack propagation proceeding in a fully automatic way.

## References

- [1] R.S. Mishra, Z.Y. Ma, “Friction stir welding and processing”, *Materials Science and Engineering: R*, 50, 1-78, 2005.
- [2] M. Guerra, C. Schmidt, J.C. McClure, L.E. Murr, A.C. Nunes, “Flow patterns during friction stir welding”, *Materials Characterization*, 49, 95-101, 2003.
- [3] V. Balasubramanian, “Relationship between base metal properties and friction stir welding process parameters”, *Materials Science & Engineering A*, 480, 397-403, 2008.
- [4] M.A. Sutton, B. Yang, A.P. Reynolds, R. Taylor, “Microstructural studies of friction stir welds in 2024-T3 aluminum”, *Materials Science & Engineering A*, 323, 160-166, 2002.
- [5] H.J. Liu, H. Fujii, M. Maeda, K. Nogi, “Tensile properties and fracture locations of friction-stir-welded joints of 2017-T351 aluminum alloy”, *Journal of Materials Processing Technology*, 142, 692-696, 2003.
- [6] J.-Q. Su, T.W. Nelson, R. Mishra, M. Mahoney, “Microstructural investigation of friction stir welded 7050-T651 aluminium”, *Acta Materialia*, 51, 713-729, 2003.
- [7] A. Abdollah-Zadeh, T. Saeid, B. Sazgari, “Microstructural and mechanical properties of friction stir welded aluminum/copper lap joints”, *Journal of Alloys and Compounds*, 460, 535-538, 2008.

- [8] T. Watanabe, H. Takayama, A. Yanagisawa, "Joining of aluminum alloy to steel by friction stir welding", *Journal of Materials Processing Technology*, 178, 342-349, 2006.
- [9] A. Kostka, R.S. Coelho, J. dos Santos, and A.R. Pyzallac, "Microstructure of friction stir welding of aluminium alloy to magnesium alloy", *Scripta Materialia*, 60, 953-956, 2009.
- [10] P.M.G.P. Moreira, A.M.P. de Jesus, A.S. Ribeiro, P.M.S.T. de Castro, "Fatigue crack growth in friction stir welds of 6082-T6 and 6061-T6 aluminium alloys: A comparison", *Theoretical and Applied Fracture Mechanics*, 50, 81-91, 2008.
- [11] P.M.G.P. Moreira, F.M.F. de Oliveira, P.M.S.T. de Castro, "Fatigue behavior of notched specimens of friction stir welded aluminium alloy 6063-T6", *Journal of Materials Processing Technology*, 207, 283-292, 2008.
- [12] L. Fratini, S. Pasta, A.P. Reynolds, "Fatigue crack growth in 2024-T351 friction stir welded joints: Longitudinal residual stress and microstructural effects", *International Journal of Fatigue*, 31, 495-500, 2009.
- [13] S. Kainuma, H. Katsuki, I. Iwai, M. Kumagai, "Evaluation of fatigue strength of friction stir butt-welded aluminum alloy joints inclined to applied cyclic stress", *International Journal of Fatigue*, 30, 870-876, 2008.
- [14] O. Hatamleh, "A comprehensive investigation on the effects of laser and shot peening on fatigue crack growth in friction stir welded AA 2195 joints", *International Journal of Fatigue*, 31, 974-988, 2009.
- [15] E. Armentani, R. Esposito, R. Sepe, "The influence of thermal properties and preheating on residual stresses in welding", *International Journal of Computational Materials Science and Surface Engineering*, 1(2), 146-162, 2007.
- [16] H.W. Zhang, Z. Zhang, J.T. Chen, "The finite element simulation of the friction stir welding process", *Materials Science and Engineering A*, 403, 340-348, 2005.
- [17] M. Peel, A. Stewer, M. Preuss, P.J. Withers, "Microstructure, mechanical properties and residual stress as a function of welding speed in aluminium AA5083 friction stir welds", *Acta Materialia*, 51, 4791-4801, 2003.
- [18] W. Xu, J. Liu, H. Zhu, "Analysis of residual stresses in thick aluminum friction stir welded butt joints", *Materials & Design*, 32, 2000-2005, 2011.
- [19] Mi, Y., Aliabadi, M.H., "Dual Boundary Element Method for Three Dimensional Fracture Mechanics Analysis", *Engineering Analysis with Boundary Elements*, 10, 161-171, 1992.
- [20] M K. Sadananda, A.K. Vasudevan, "Short crack growth and internal stresses", *International Journal of Fatigue* 19, S99-S108, 1997.
- [21] C. Hamilton, S. Dymek, M. Blicharski, "A model of material flow during friction stir welding", *Materials Characterization*, 59, 1206-1214, 2008.
- [22] M.B. Prime, "Cross-sectional mapping of residual stresses by measuring the surface contour after a cut", *Journal of Engineering Materials and Technology*, 123, 162-168, 2001.
- [23] P. Rangaswamy, M.L. Griffith, M.B. Prime, T.M. Holden, R.B. Rogge, J.M. Edwards, R.J. Sebring, "Residual stresses in LENS<sup>®</sup> components using

- neutron diffraction and contour method”, *Materials science and Engineering A*, 399, 72-83, 2005.
- [24] D. Thibault, P. Bocher, M. Thomas, M. Gharghour, M. Côté, “Residual stress characterization in low transformation temperature 13%Cr-4%Ni stainless steel weld by neutron diffraction and the contour method”, *Materials Science and Engineering A*, 527, 6205-6210, 2010.
- [25] M.E. Kartal, C.D.M. Liljedahl, S. Gungor, L. Edwards, M.E. Fitzpatrick, “Determination of the profile of the complete residual stress tensor in a VPPA weld using the multi-axial contour method”, *Acta Materialia*, 56, 4417-4428, 2008.
- [26] P. Carlone, G.S. Palazzo, “Experimental analysis of the influence of the process parameters on residual stress in AA2024-T3 friction stir welds”, *Key Engineering Materials*, 504-506, 753-758, 2012.
- [27] R. Citarella, G. Cricri, “A two-parameter model for crack growth simulation by combined FEM-DBEM approach”, *Advances in Engineering Software*, 40, 363-373, 2009.